Creating and Stabilizing an Oxidized Pd Surface under Reductive Conditions for Photocatalytic Hydrogenation of Aromatic Carbonyls

Published Version:
Creating and Stabilizing an Oxidized Pd Surface under Reductive Conditions for Photocatalytic Hydrogenation of Aromatic Carbonyls / Qiao, Wei; Fan, Xing; Liu, Weifeng; Khan, Fahir Niaz; Zhang, Dongsheng; Han, Feiyu; Yue, Huiyu; Li, Yajiao; Dimitratos, Nikolaos; Albonetti, Stefania; Wen, Xiaodong; Yang, Yong; Besenbacher, Flemming; Li, Yongwang; Niemantsverdriet, Hans; Lin, Haiping; Su, Ren. - In: JOURNAL OF THE AMERICAN CHEMICAL SOCIETY. - ISSN 1520-5126. - ELETTRONICO. - 145:9(2023), pp. 5353-5362. [10.1021/jacs.2c13196]

Availability:
This version is available at: https://hdl.handle.net/11585/925017 since: 2023-05-09

Published:
DOI: http://doi.org/10.1021/jacs.2c13196

Creating and Stabilizing an Oxidized Pd Surface under Reductive Conditions for Photocatalytic Hydrogenation of Aromatic Carbonyls

Wei Qiao[1,2‡], Xing Fan[3‡], Weifeng Liu[4‡], Fahir Niaz Khan[1], Dongsheng Zhang[1,2], Feiyu Han[1,2], Huiyu Yue[1], Yajiao Li[1], Nikolaos Dimitratos[4,5], Stefania Albonetti[4,5], Xiaodong Wen[2,6], Yong Yang[2,6], Flemming Besenbacher[7], Yongwang Li[2,6], Hans Niemantsverdriet[2,8], Haiping Lin[9,*], Ren Su[1,2,*]

[1] Soochow Institute for Energy and Materials Innovations (SIEMIS), Soochow University, Suzhou, 215006, China

[2] SynCat@Beijing, Synfuels China Technology Co. Ltd., Leyuan South Street II, No.1, Beijing, 101407, China

[3] Research Center for Carbon-based Electronics and Key Laboratory for the Physics and Chemistry of Nanodevices, School of Electronics, Peking University, Beijing 100871, China

[4] Dipartimento di Chimica Industriale "Toso Montanari", University of Bologna, Bologna 40136, Italy

[5] Center for Chemical Catalysis-C3, Alma Mater Studiorum University of Bologna, Bologna 40136, Italy

[6] State Key Laboratory of Coal Conversion, Institute of Coal Chemistry, CAS, Taiyuan, 030001, China

[7] The Interdisciplinary Nanoscience Center (iNANO), Aarhus University, DK-8000 Aarhus, Denmark

[8] SynCat@DIFFER, Syngaschem BV, 6336 HH Eindhoven, The Netherlands

[9] School of Physics and Information Technology, Shaanxi Normal University, Xi'an, 710119, China

ABSTRACT: Photocatalysis provides an eco-friendly route for the hydrogenation of aromatic carbonyls to O-free aromatics, which is an important refining process in the chemical industry that is generally carried out under high pressure of hydrogen at elevated temperatures. However, aromatic carbonyls are often only partially hydrogenated to alcohols, which readily desorbs and are hardly further deoxygenated under ambient conditions. Here we show that by constructing an oxide surface over the Pd cocatalyst supported on graphitic carbon nitride, an alternative hydrogenation path of aromatic carbonyls becomes available via a step-wise acetalization and hydrogenation, thus allowing efficient and selective production of O-free aromatics. The PdO surface allows for optimum adsorption of reactants and intermediates and rapid abstraction of hydrogen from the alcohol donor, favoring fast acetalization of the carbonyls and their consecutive hydrogenation to O-free hydrocarbons. The photocatalytic hydrogenation of benzaldehyde into toluene shows a high selectivity of >90% and a quantum efficiency of ~10.2% under 410 nm irradiation. By adding trace amounts of HCl to the reaction solution, the PdO surface remains stable and active for long-term operation at high concentrations, offering perspective for practical applications.

INTRODUCTION

Catalytic reduction of unsaturated C=O bonds in aromatic hydrocarbons is of crucial importance in the processing of coal and petrochemicals, the upgrading of biomass, and in the pharmaceutical industries.[1-4] In comparison with the Clemmensen or the Wolff−Kishner reductions that require toxic Hg as the catalyst or hazardous hydrazine as the reductant, supported Pd catalysts can hydrogenate carbonyl groups into methyl groups under relatively eco-friendly reaction conditions, though pressurized hydrogen and high temperature are still required.[5-6] To avoid over-reduction of other unsaturated bonds and damaging of special functional groups, precise design of the catalyst and careful control over the reaction conditions are required to achieve a high selectivity towards the aimed products.[7-9] Heterogeneous photocatalysis employing noble metal cocatalysts (*i.e.*, Au, Pd, Pt) is capable of deprotonating bio-mass derived liquid hydrogen donors (*i.e.*, alcohols, acids and amines) to produce atomic hydrogen species under solar irradiation and ambient atmosphere, thus offering a mild hydrogenolysis platform for the reduction of aromatic carbonyl compounds.[10-13] However, often aromatic alcohol species are observed as the final products (*e.g.*, benzyl alcohol) instead of the desired O-free hydrocarbons (*e.g.*, toluene),[14-16] limiting the use of photocatalysis for practical applications.

Two pathways exist for the photocatalytic hydrogenation of carbonyl groups into methyl groups in aromatic compounds using alcohol as the hydrogen donor, as shown for benzaldehyde and ethanol as the model reactants in Scheme 1a. The commonly considered route is *via* the formation of an aromatic alcohol intermediate with two H atoms abstracted from the sacrificial alcohol donor (Path I). The aromatic alcohol is then further hydrogenated with two additional H atoms into an O-free aromatic. The alternative, though seldomly reported, is *via* the formation of an acetal, which is subsequently hydrogenated into the final product (Path II). Note that while the hydrogenation of acetal is a photocatalytic process, the formation of acetal intermediates does not involve any redox reaction and can be realized *via* acidic catalysis.[17-19] Thermodynamics indicates that the hydrogenation of benzaldehyde into toluene *via* either pathway is energetically downhill (Scheme 1b). Ideally, a photocatalyst modified with metal cocatalysts (*i.e.*, Pd, Pt, Ni) that are efficient in hydrogen abstraction from the alcohol donors and hydrogenation of the aromatic carbonyls can realize such process *via* path I. However, aromatic alcohols generated *via* Path I are the most frequently reported final products,[20-22] whereas the more thermodynamically stable O-free aromatics are rarely observed, with few exceptions.[21] In contrast, though the formation of acetal intermediates is observed using pristine TiO_2 under irradiation,[23] the photocatalytic hydrogenation of aromatic carbonyls to the O-free aromatics *via* Path II has not been reported, though such process may provide a high selectivity.

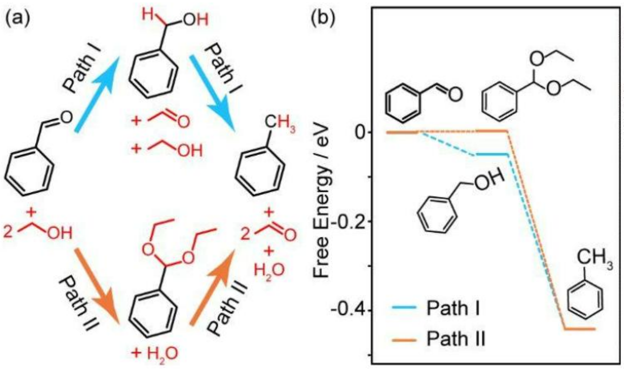

Scheme 1. Photocatalytic hydrogenation of aromatic carbonyls. (a) Reaction pathways for the conversion of benzaldehyde into toluene *via* benzyl alcohol (Path I) and *via* diacetal (Path II) employing ethanol as the hydrogen donor. (b) Calculated free energies of benzyl alcohol, benzaldehyde diethyl acetal, and toluene relative to benzaldehyde.

We consider that the surface chemical state of the metal cocatalysts under realistic photocatalytic reaction conditions dictate its interaction with the aromatic carbonyls and intermediates, especially for organic transformations under ambient conditions.[24-26] Among transition metals, Pd is the most often employed catalyst for hydrogenation reactions,[27-29] owing to its optimized adsorption of the hydrogen acceptors and hydrogen atoms. The Pd nanostructures are also decent cocatalysts in photocatalytic hydrogen atom transfer (HAT) reactions due to its fast hydrogen abstraction and donation kinetics.[30-31] Under such hydrogen rich conditions, metallic and hydrogenated Pd nanoparticles (NPs) are often observed as the stable catalyst.[32-33] In contrast, creating and stabilizing an oxidized surface of the Pd cocatalyst under a reductive environment remains a challenge and has been barely reported.

Herein, we show that the photocatalytic hydrogenation pathways and products of aromatic carbonyls can be tuned by tweaking the surface oxidation states of the Pd NPs supported on the photocatalyst. While the partially hydrogenated Pd NPs on graphitic carbon nitride (PdH_X/CN) promote direct photocatalytic hydrogenolysis of aromatic carbonyls to the corresponding alcohols, photocatalytic conversion into oxygen-free aromatic hydrocarbons can be realized *via* an indirect acetalization process by anchoring surface oxidized Pd NPs on $g\text{-}C_3N_4$ [Pd(II)/CN]. By adding trace amounts of HCl to the reaction system, the Pd(II)/CN photocatalyst presents a stabilized high activity for the conversion of a series of aromatic carbonyls to the corresponding O-free aromatics, rendering it a promising process for scaling-up.

RESULTS AND DISCUSSION

Theoretical predictions. We have first explored the free adsorption energies of possible intermediates on metallic Pd, partially hydrogenated Pd ($Pd_{36}H_9$), and oxidized Pd surface in the hydrogenation of benzaldehyde with ethanol molecules in presence on the surface (Figure 1, Supplementary Note 1, and Supplementary Figures 1-3). While a strong adsorption of benzaldehyde is observed on a metallic Pd surface (-0.86 eV), the hydrogenated Pd surface presents a weakened interaction with benzaldehyde (-0.55 eV). The strong adsorption energy of toluene on metallic Pd (-1.19 eV) also renders it a poor cocatalyst for such process, in particular for reactions proceed at room temperature (RT). In comparison, the PdO surface exhibits an optimum adsorption energy of benzaldehyde (-0.06 eV, Figures 1a and 1b). Additionally, benzaldehyde diethyl acetal, benzyl alcohol and toluene, all present a weak-to-medium adsorption on the PdO surface (-0.09, -0.14 and -0.53 eV, Figures 1b-1e), revealing that the hydrogenation of benzaldehyde with ethanol is a thermo-dynamically favorable process under ambient conditions on the PdO surface. The very weak adsorption of benzaldehyde diethyl acetal on PdO also implies that it may appear as an observable intermediate in the liquid phase prior to the formation of toluene. In comparison, while benzyl alcohol does not adsorb on the partially hydrogenated Pd surface (0.15 eV), benzaldehyde diethyl acetal adsorbs too strong on the $Pd_{36}H_9$ surface (-1.33 eV). Considering the relatively strong adsorption energy of toluene on $Pd_{36}H_9$ (-0.87 eV), it implies that the partially hydrogenated alcoholic species will desorb into the liquid phase as the final product. Moreover, the adsorption of ethanol on PdO (-1.27 eV) is relatively strong than Pd (-0.90 eV) and $Pd_{36}H_9$ (-0.74 eV), implying that the acetalization of adsorbed benzaldehyde is more feasible on the PdO surface (Supplementary Table 1).

Pd decorated photocatalysts. The Pd NPs with controllable chemical states were deposited on the $g\text{-}C_3N_4$ photocatalyst (gCN) using a modified photo-deposition method by adjusting the alcohol concentration and irradiation time (Figure 2a and Supplementary Note 2). For the synthesis of Pd(II)/CN, the $PdCl_2$ precursor and the $g\text{-}C_3N_4$ (gCN) powders were dispersed in an aqueous ethanol solution (67 vol%) and irradiated for 5 h under deaerated conditions. The preparation of PdH_X/CN was performed in absolute ethanol (>99.7 vol%) using a prolonged irradiation time (10 h) to create reduced Pd NPs with a partially hydrogenated surface. Both Pd(II)/CN and PdH_X/CN had a Pd loading of ~3 wt%.

The two photocatalysts were characterized by inductively coupled plasma atomic emission spectroscopy (ICP-AES), X-ray photoelectron spectroscopy (XPS), electrochemical cyclic voltammetry (CV), X-ray diffraction (XRD), and transmission electron microscopy (TEM), as shown in Supplementary Figures 4-9 and Supplementary Table 2. While the PdH_X/CN contains exclusively metallic Pd species according to the XPS Pd3d spectra (Pd^0, ~335 eV, Figure 2b), both Pd^0 and Pd^{2+} of PdO (~337 eV) are present in Pd(II)/CN. The CV analysis of PdH_X/CN displays a pair of redox peaks corresponding to the evolution of molecular hydrogen from PdH_X and adsorption of atomic hydrogen on Pd^0 back to PdH_X (Figure 2c).[34-37] In comparison, no obvious redox peaks are observed for Pd(II)/CN. The XRD patterns of both samples reveal that the bulk metallic Pd NPs are in the cubic phase and the gCN remains as is after photo-deposition (Supplementary Figure 7). The Pd (111) diffraction peak for PdH_X/CN becomes broaden and is shifted to a lower 2θ angle (39.8°) compared to that of the Pd(II)/CN, indicating a reduced long-range order of the Pd nanocrystalline caused by a high degree of hydrogenation of Pd NPs within the PdH_X/CN.[38-39] In contrast, the Pd NPs in Pd(II)/CN are covered by a thin oxide layer on the surface of bulk metallic Pd according to XRD and XPS analysis.

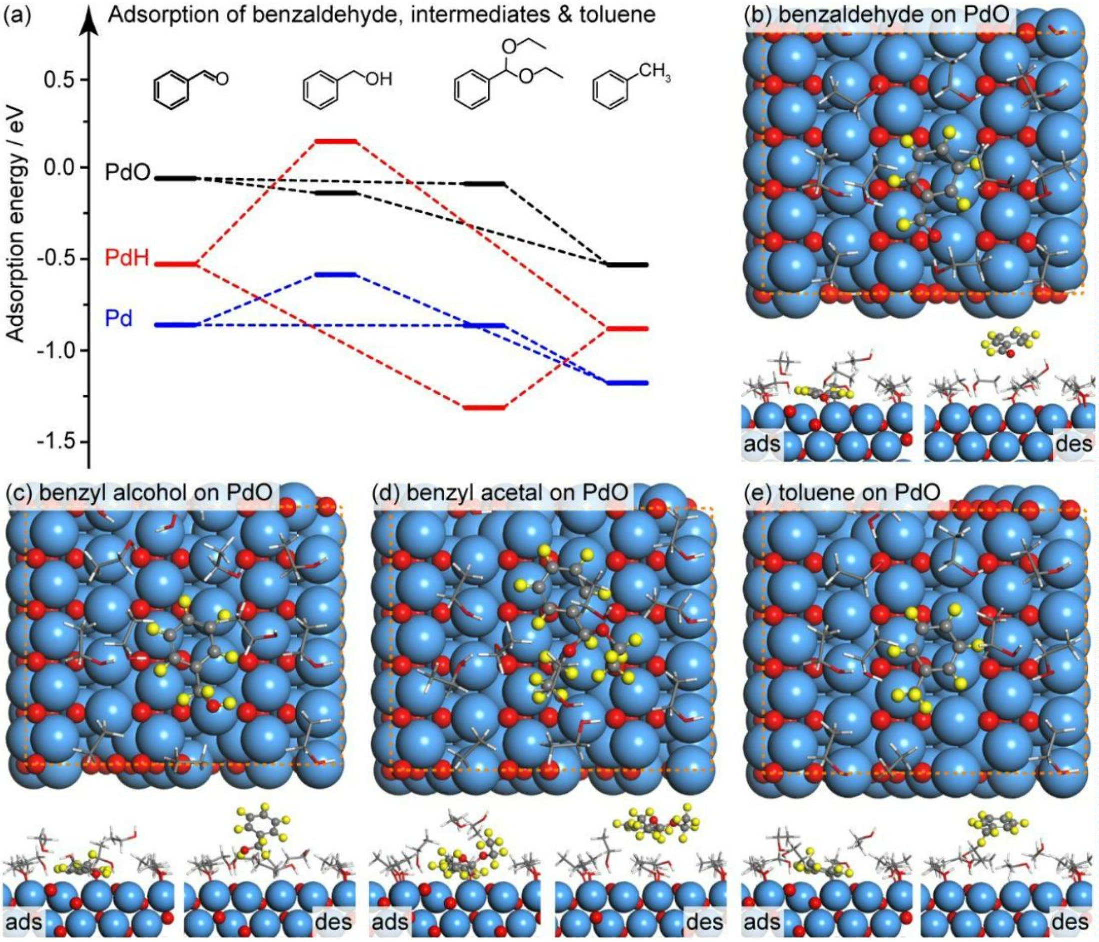

Figure 1. Adsorption of key chemicals on different Pd surfaces. (a) Relative energy profiles of reactant, intermediates, and products in photocatalytic hydrogenation of benzaldehyde in ethanol on Pd, $Pd_{36}H_9$, and PdO, respectively. (b)-(e) Adsorption models of benzaldehyde, benzyl alcohol, benzaldehyde diethyl acetal, and toluene with ten ethanol molecules on PdO surface.

Temperature programmed desorption (TPD) reveals that a large quantity of benzaldehyde is weakly adsorbed on Pd(II)/CN photocatalyst with a desorption peak at ~81 °C (Figure 2d), whereas a reduced quantity of benzaldehyde is adsorbed on PdH_X/CN with a stronger affinity (desorption peak at ~151 °C). Additionally, benzaldehyde diethyl acetal and benzyl alcohol are also weakly adsorbed on Pd(II)/CN with desorption peaks located at ~87 °C and 105 °C, respectively (Supplementary Figure 10), all agreeing qualitatively with the theoretical prediction. The limited adsorption of acetal on Pd(II)/CN in quantity implies that it is likely to diffuse into the liquid phase during photocatalytic hydrogenation of benzaldehyde, which results in higher availability of sites for the adsorption and acetalization of benzaldehyde. The adsorption of benzaldehyde on pristine graphitic carbon nitride is negligible (Supplementary Figure 10).

TEM imaging reveals that the as-synthesized Pd NPs in Pd(II)/CN are relatively large (average diameter ~16.4 nm with a broader distribution; Figures 2e, 2f and Supplementary Figures 9a, 9b). The Pd particles develop a well-crystalline structure with a lattice spacing of 0.22 nm in the bulk that matches well with that of Pd (111), according to the high-resolution TEM image (HRTEM, Figure 2g), while the surface consists of an amorphous layer that is most likely to be PdO. In comparison, the PdH_X NPs (averaged size ~ 4.9 nm) are homogeneously dispersed on the gCN photocatalyst (Figures 2h, 2i and Supplementary Figures 9c, 9d). HRTEM imaging on a single PdH_X particle shows that it contains disordered (dashed-line bordered areas) and crystalline regions with a lattice spacing of 0.23 nm, close to that of Pd (111) facet (Figure 2j). The smaller particle size of Pd in PdH_X/CN indicates that the hydrogen adsorption results in breaking of the Pd NPs into smaller clusters. This is in good agreement with the XRD pattern of the PdH_X/CN, confirming the H-induced disordering in Pd NPs.[40]

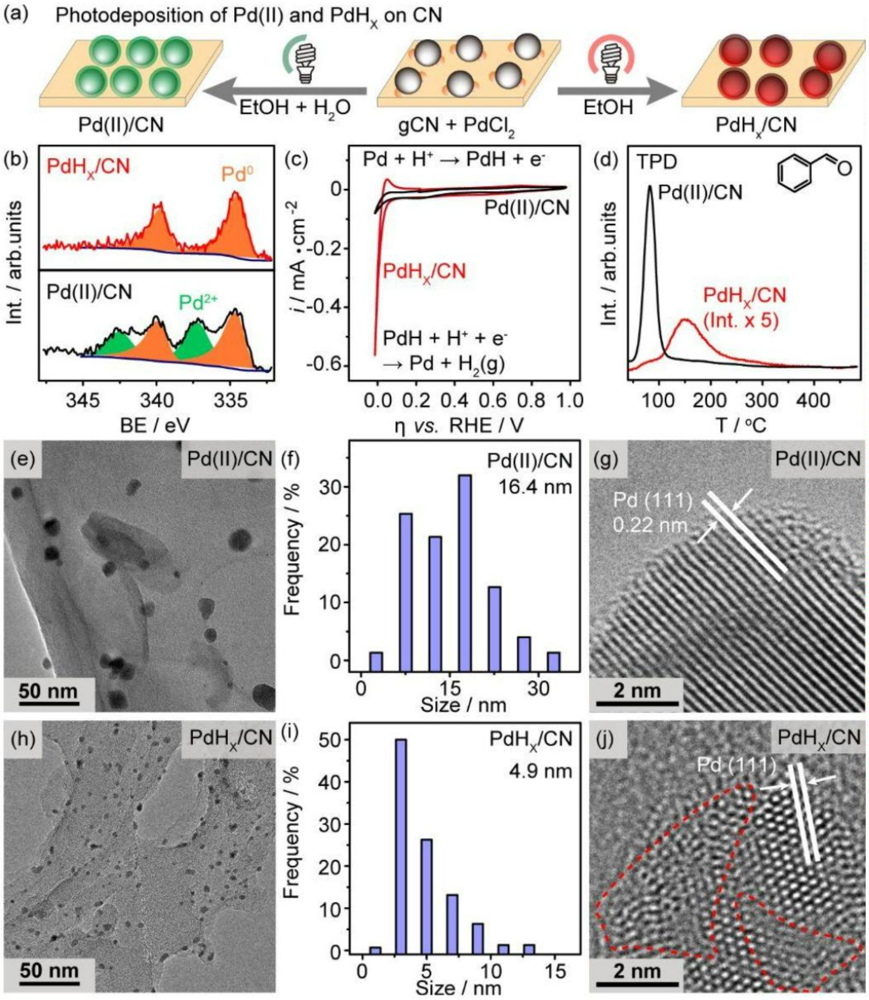

Figure 2. Catalyst synthesis & characterizations. (a) Scheme of the photo-assisted synthesis of Pd(II)/CN and PdH_X/CN. (b) and (c) XPS and CV analysis of Pd(II)/CN and PdH_X/CN, respectively. The CV was performed in 0.5 M H_2SO_4 with a three-electrode system with the catalyst on glassy carbon, a graphitic carbon sheet, and Ag|AgCl as the working, counter, and reference electrodes, respectively. (d) TPD of benzaldehyde from Pd(II)/CN and PdH_X/CN. (e)-(j) TEM, particle size distribution, and HRTEM images of the Pd NPs within the Pd(II)/CN and PdH_X/CN.

Photocatalytic performance. Photocatalytic hydrogenation of benzaldehyde is employed as the model reaction to evaluate the performance of Pd(II)/CN and PdH_X/CN photocatalysts under deaerated conditions at RT in ethanol, which serves both as solvent and as hydrogen donor. The time sequence for Pd(II)/CN is characterized by a series of consecutive reactions where the rate of product formation is substantially larger than for the intermediate (Figure 3a).[41] Benzaldehyde (black) rapidly reacts with ethanol to benzaldehyde diethyl acetal (red) in the initial stage (< 5 min) and eventually to toluene within 50 min of irradiation. Relatively small amounts of benzyl alcohol (blue) and phenyl ethyl ether (olive) appear at intermediate times (Figure 3a). Note that benzaldehyde also converts into acetal under dark but at a slower rate in the presence of Pd(II)/CN, indicating that the acetalization is indeed promoted by irradiation. This is likely a heat-induced acidic catalytic acetalization driven by the localized surface plasmonic resonance of the Pd NPs rather than a photocatalytic redox reaction (Supplementary Table S3). As the irradiation proceeds, the generated acetal intermediate gradually converts to toluene *via* a deoxygenation and hydrogenation steps. Noteworthy, the minor intermediates (benzyl alcohol, phenyl ethyl ether) also gradually hydrogenated, resulting in a high yield of toluene (>90%). This corresponds to a high quantum efficiency (QE) of ~10%, as one part of benzaldehyde requires four hydrogen atoms to produce a toluene molecule (Supplementary Note 3). The hydrogenation of benzaldehyde to toluene can be realized under a wide range of reaction conditions (*i.e.*, loading of Pd, concentration of photocatalyst, and irradiation wavelength, Supplementary Figure 11).

In comparison, the PdH_X/CN selectively converts benzaldehyde to benzyl alcohol without the formation of acetal and toluene even after prolonged radiation (Figure 3b). The time dependence indicates zeroth-order reaction kinetics, which is usually associated with strong adsorption of the reactant on the catalyst. This agrees well with the theoretical calculation of the adsorption energy, where the optimum interaction of acetal and toluene with the oxidized Pd surface is the key to liberate the intermediate and the final hydrogenated product.

The photocatalytic hydrogenation pathway is further analyzed using benzaldehyde diethyl acetal as the initial reactant under deaerated conditions in ethanol. The Pd(II)/CN rapidly and completely hydrogenates the diacetal, possibly *via* phenyl ethyl ether to toluene within 30 mins of irradiation (Figure 3c). The absence of benzyl alcohol indicates that hydrolysis of the acetal does not occur under these ethanol-rich conditions. No reaction of the diacetal is observed for the PdH_X/CN (Figure 3d), matching well to the calculated strong adsorption of diacetal and toluene on the hydrogenated Pd surface. Note that benzyl alcohol readily converts to toluene on Pd(II)/CN when in presence (Figure 3e), although it appears as a minor route in the hydrogenation of benzaldehyde.

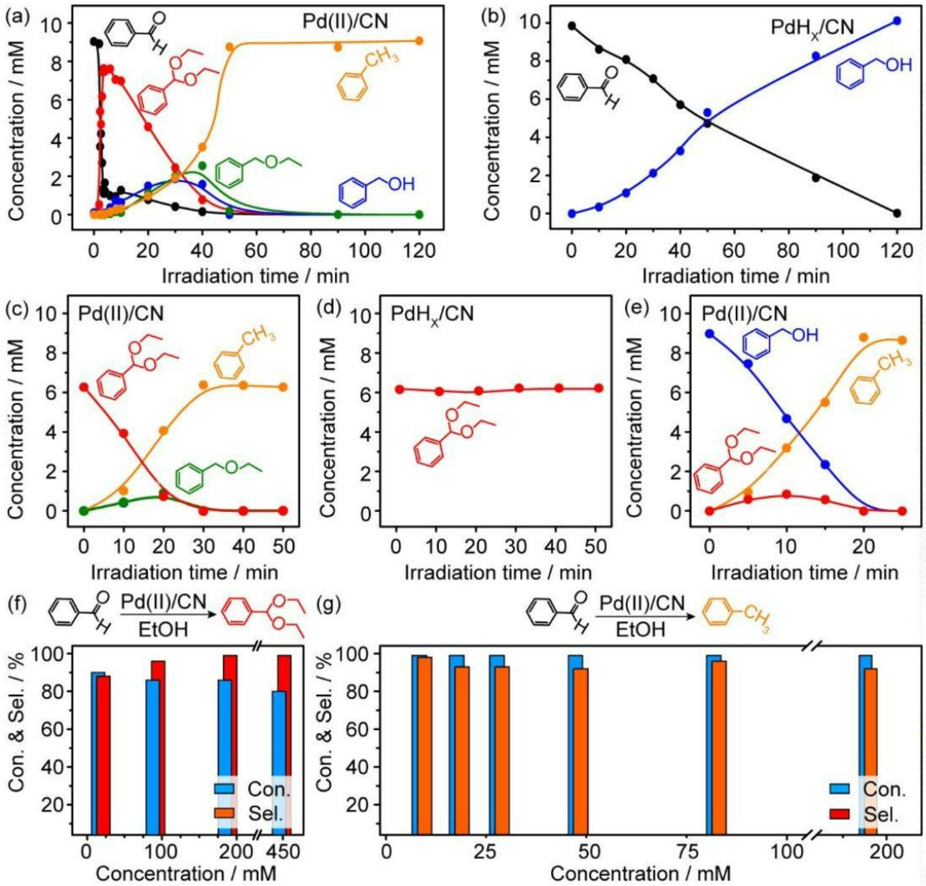

Figure 3. Photocatalytic performances. (a)-(e) Time courses of photocatalytic hydrogenation of benzaldehyde, benzaldehyde diethyl acetal and benzyl alcohol using Pd(II)/CN and PdH_X/CN; reaction conditions: 10 mg photocatalyst with reactants in 2 mL ethanol under 410 nm irradiation (14.8 mW·cm^{-2}) in Ar at RT. (f) and (g) Effect of starting concentrations of benzaldehyde for the synthesis of diethyl acetal and toluene using Pd(II)/CN.

Photocatalytic hydrogenation of benzaldehyde to toluene *via* the acetalization path using Pd(II)/CN remains applicable and efficient even at higher concentrations of reactants (Figures 3f and 3g). For the intermediate benzaldehyde diethyl acetal, a satisfactory selectivity is achieved by prolonging the irradiation time with the initial concentration of benzaldehyde (15 min for 90 mM, 35 min for 180 mM, and 75 min for 450 mM). The hydrogenation of benzaldehyde into toluene at elevated concentrations (20, 30, 50, 80 and 190 mM) can also be realized with high conversion (> 95%) and selectivity (> 90%) by extending the radiation time to 2, 3, 4, 6, and 24 h, respectively, suggesting promising potential for applications. Finally, the hydrogenation of benzaldehyde to toluene is also realized using glycerol, a low-cost byproduct in biomass conversion, as the hydrogen donor (Supplementary Figure 12).

Stability & reusability. Since noble metal oxides generally reduce under hydrogen-rich conditions, the sustainability of the Pd(II)/CN photocatalyst for the hydrogenation of aromatic aldehydes and ketones in pure ethanol upon prolonged irradiation should be considered and examined prior to practical applications. The CVs of the pre-irradiated Pd(II)/CN in pure ethanol for 3 and 9 h display a pair of redox peaks that are similar to that of the fresh PdH_X/CN (Figure 4a), suggesting that the oxide layer of Pd NPs in Pd(II)/CN has been converted into a hydride surface. XPS analysis of the spent Pd(II)/CN photocatalyst further confirms the reduction of oxidic Pd surface upon irradiation in pure ethanol (Figure 4b). The content of Pd^{2+} species decreases from 33 at% in the fresh Pd(II)/CN down to 17 at% after 3 h of irradiation and eventually to 5 at% after 9 h of irradiation in pure ethanol, resulting in a gradual deactivation of the photocatalyst and alternation of the reaction paths (Figure 4c). The Pd(II)/CN photocatalyst shows a high conversion of benzaldehyde into toluene within the first two cycles, however the selectivity to toluene gradually decreases and the evolution of benzyl alcohol becomes dominant after the 5th cycle. The selectivity to benzyl alcohol increases to 90% after the 7th cycle (Supplementary Figure 13), indicating complete reduction of the Pd^{2+} species in Pd(II)/CN after prolonged use.

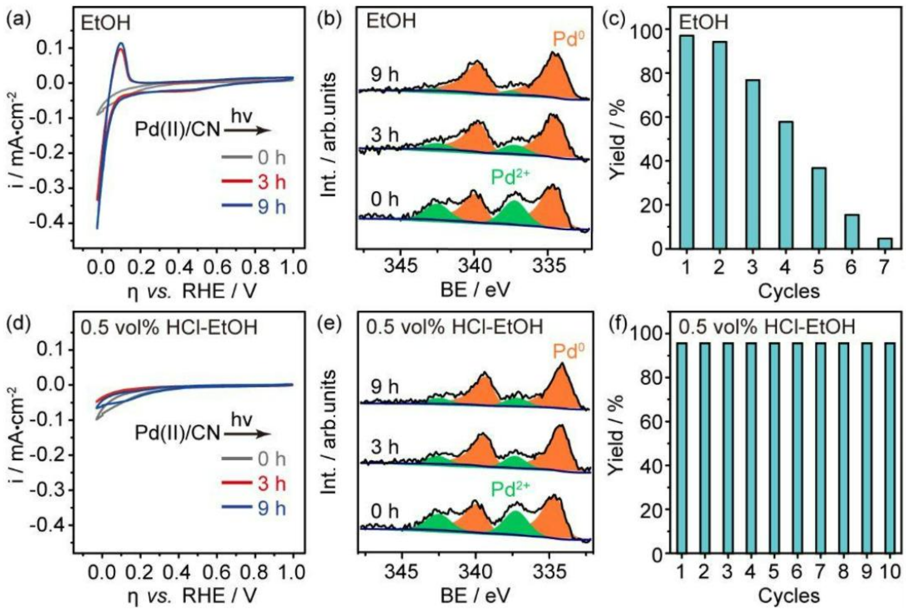

Figure 4. Stability & Reusability. (a) and (b) CV and Pd3d XPS of the Pd(II)/CN photocatalyst after irradiation for 3 and 9 h in ethanol. Spectra for the fresh Pd(II)/CN are included for comparison. (c) Reusability of Pd(II)/CN for photocatalytic hydrogenation of benzaldehyde to toluene in pure ethanol. (d) and (e) CV and Pd3d XPS of the Pd(II)/CN photocatalyst after irradiation for 3 and 9 h in a 0.5 vol% HCl-ethanol solution. (f) Reusability of Pd(II)/CN for photocatalytic hydrogenation of benzaldehyde to toluene in a 0.5 vol% HCl-ethanol solution.

The Pd oxide layer can be stabilized by adding small amounts of HCl to the reaction solution. Figure 4d shows the CVs of irradiated Pd(II)/CN samples in a 0.5 vol% HCl-ethanol solution, where no redox peaks related to the PdH_X species are observed even after irradiation for 9 h. Accordingly, the concentration of Pd^{2+} species remains at ~16 at% up to a irradiation time of 9 h, although a small fraction of the material has been reduced compared to the fresh Pd(II)/CN (Figure 4e). The Pd(II)/CN exhibits high conversion of benzaldehyde to toluene in photocatalytic hydrogenation in a 0.5 vol% HCl-ethanol solution for 10 consecutive cycles, confirming the surface Pd oxide layer is well preserved (Figure 4f). TEM imaging of the spent Pd(II)/CN photocatalyst reveals that most Pd NPs remain well-crystalline, although the average particle size is reduced to 5.6 nm (Supplementary Figures 14a-14f). XPS analysis of the spent catalyst indicates that the addition of HCl during reaction does not result in deposition of Cl species on the catalyst (Supplementary Figures 14g and 14h).

Reaction mechanisms. We have further investigated the hydrogenation of aromatic carbonyls on Pd(II)/CN by *in-situ* mass spectrometry (MS, Supplementary Note 4). In the absence of a hydrogen acceptor (*e.g.*, benzaldehyde), molecular hydrogen evolves from the Pd(II)/CN upon irradiation in pure ethanol (black curve, Figure 5a), while 1,1-diethoxy ethane appears in solution. In contrast, the PdH_X/CN shows negligible hydrogen evolution under identical reaction conditions (red curve, Figure 5a), while no 1,1-diethoxy ethane evolves in the liquid. This indicates that the PdO layer in the Pd(II)/CN system facilitates the cleavage of the C-H bond in ethanol, whereas the PdH_X/CN photocatalyst cannot catalyze the dehydrogenation of ethanol into acetaldehyde and the consecutive acetalization. Both photocatalysts exhibit a delayed H_2 evolution upon irradiation when benzaldehyde is in present in the ethanol as hydrogen acceptor (Figure 5b), implying that the hydrogenation of benzaldehyde is thermodynamically more favorable than the evolution of H_2. The relatively slow kinetics of H_2 evolution from PdH_X/CN in the presence of benzaldehyde probably indicates that the H-atoms stored in PdH_X need to be depleted first to provide active sites for the dehydrogenation of ethanol.

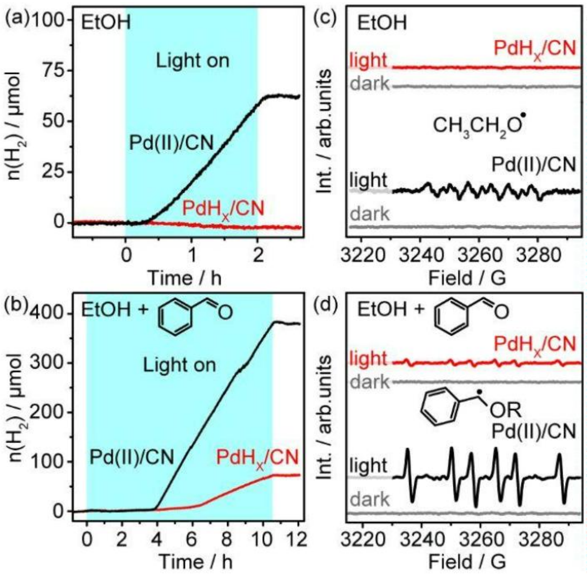

Figure 5. Reaction mechanisms. (a)-(d) *in-situ* MS analysis of H_2 evolution and ESR analysis of radical species under irradiation using Pd(II)/CN and PdH_X/CN photocatalysts, respectively. Reaction conditions: 10 mg photocatalyst in 2 mL of pure ethanol and with 10 mM benzaldehyde in ethanol under 410 nm irradiation (14.8 $mW\cdot cm^{-2}$) under Ar atmosphere at RT. DMPO is used as the spin trap for ESR analysis.

Electron spin resonance (ESR) is used to study the possible radical species evolved during photocatalytic hydrogenation of benzaldehyde using 5,5-dimethyl-1-pyrroline N-oxide (DMPO) as the spin trap. No radical species were detected under dark conditions regardless of the photocatalyst and reactants, confirming that the hydrogenation of benzaldehyde into either benzyl alcohol or toluene using PdH_X/CN and Pd(II)/CN, respectively, is indeed a photocatalytic process. While Pd(II)/CN produces detectable O-centered ethoxy radicals ($CH_3CH_2O\cdot$, $\alpha N = 13.8$, $\alpha H = 7.6$) upon irradiation in pure ethanol[42], the PdH_X/CN shows no ESR signal under identical reaction conditions (Figure 5c). This agrees with the *in-situ* MS analysis, confirming that the oxide layer over the Pd NPs is crucial in accelerating the C-H bond cleavage of ethanol to produce sufficient atomic hydrogen for the hydrogenation of benzaldehyde.

Table 1. Substate scope. Hydrogenation of aromatic carbonyls and acetalization of aldehydes with different alcohols using the Pd(II)/CN photocatalysts.

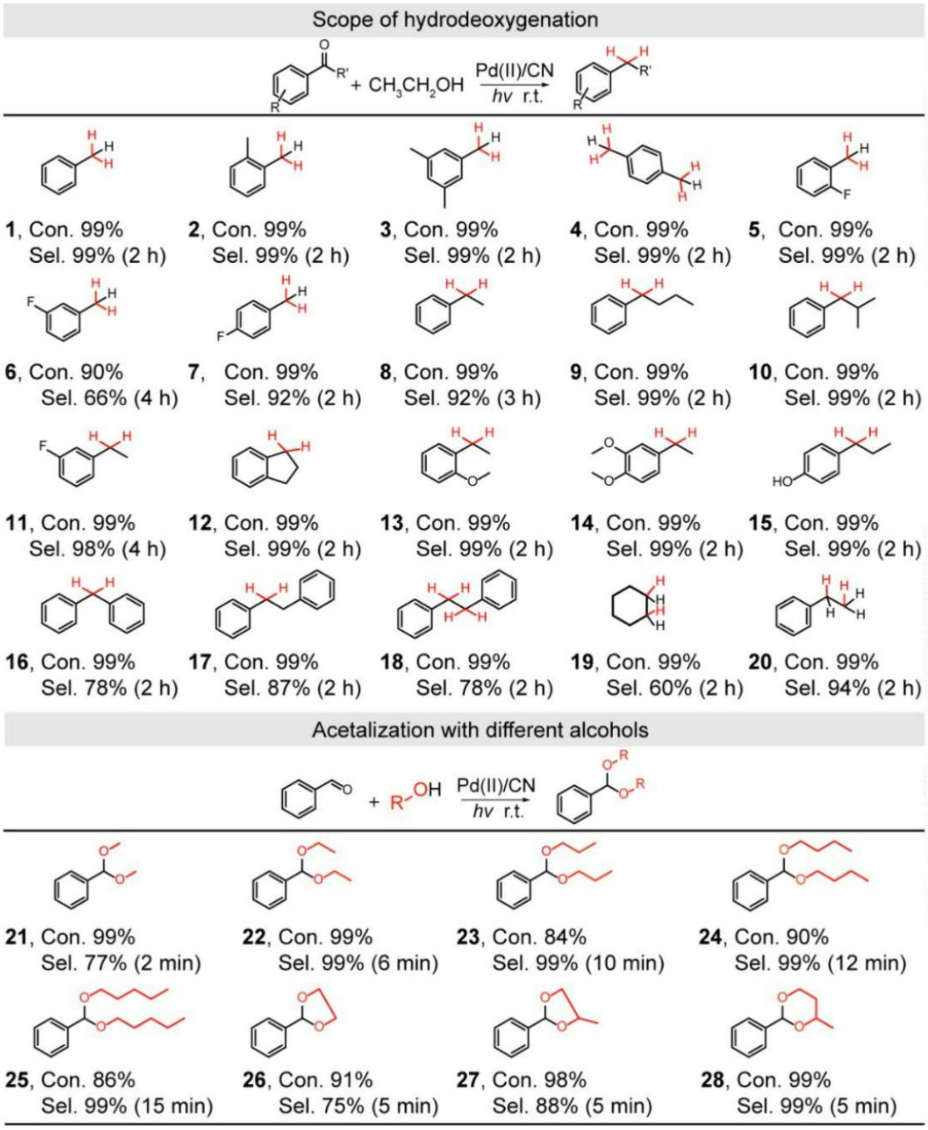

Reaction conditions: 10 mM reactant, 10 mg photocatalyst in 2 mL alcohol under 410 nm irradiation (14.8 mW·cm^{-2}) in an Ar atmosphere. The reaction time indicated in parentheses.

Substrate Scope. Finally, we show that the Pd(II)/CN photocatalyst is efficient for the hydrogenation of a series aromatic carbonyls into the corresponding O-free aromatics using ethanol as the hydrogen donor (Table 1 and Supplementary Figures 15-42). The presence of either electron donating groups (*i.e.*, $-CH_3$) or electron withdrawing groups (*i.e.*, -CHO, −F) shows a negligible impact on the selective hydrogenation of aromatic aldehydes into corresponding aromatic hydrocarbons (**2**-**7**). Noticeably, this system is also efficient and selective in hydrogenation of a series of aromatic ketones that contains methyl- (**8**), ethyl- (**9**), isopropyl- (**10**), fluoro- (**11**), cyclic- (**12**), methoxy- (**13**, **14**), hydroxyl- (**15**), and phenyl- (**16-18**) groups into the corresponding alkyl products. Also cyclohexene (**19**) and styrene (**20**) that contains unsaturated C=C bond are successfully converted to the hydrogenated products with high yields.

Additionally, the synthesis of functionalized acetals can also be realized employing a range of aliphatic alcohols and the Pd(II)/CN photocatalyst, as demonstrated using benzaldehyde as the reactant. Successful acetalization of benzaldehyde with C1-C5 primary alcohols is achieved by simply prolonging the irradiation time (**21**-**25**), offering a facial synthesis of value-added acetals under ambient conditions. Furthermore, internal acetals can be synthesized using ethylene glycol, 1,2-propanediol and 1,3-butanediol (**26**-**28**) rapidly with decent selectivity, providing an effective and environmental-friendly method for protecting the carbonyl functional group in synthetic applications.

CONCLUSIONS

In summary, we demonstrate a surface engineering strategy for rendering a Pd cocatalyst active and stable for efficient photocatalytic hydrogenation of aromatic carbonyls into O-free aromatics using alcohol as the hydrogen donor under ambient conditions. The Pd(II)/CN system consists of Pd NPs with a PdO surface supported on graphitic carbon nitride, and it catalyzes the complete hydrogenation of a series aromatic carbonyls to the corresponding aromatic hydrocarbons *via* a step-wise acetalization and hydrogenation process with acetals as the intermediate. In comparison, metallic Pd NPs occupied by H-atoms under photocatalytic reaction conditions (PdH_X) convert the aromatic carbonyls directly into aromatic alcohols as the final product. The oxide surface layer of the Pd NPs provides an ideal platform for rapid abstraction of hydrogen from the alcohol donor, acetalization of the aromatic carbonyls, subsequent hydrogenation of the acetals, and desorption of the generated aromatic hydrocarbons, and appears as an ideal cocatalyst on the semiconductor photocatalyst for complete hydrogenation. The oxide surface of the Pd NPs in the Pd(II)/CN photocatalyst can be preserved by dosing trace amount of HCl in the reaction solution to achieve an excellent stability for long term and high concentration operations, which is promising for practical applications. The approach also enables the use of bio-mass derived monohydric alcohols and polyols as eco-friendly hydrogen sources for the hydrogenation of aromatic carbonyls and the synthesis of functionalized acetals, thus offering an economic route for synthetic chemistry. The development of a suitable flow system for heterogeneous photocatalytic synthesis may be the key for scaling-up applications.

EXPERIMENTAL SECTION

Computational details. All theoretical calculations in this work were based on the periodic density functional theory (DFT) using Vienna Ab-initio Simulation Package (VASP) code.[43-44]

The electron-ion interactions were treated within the projector augmented-wave (PAW) approximation.[45-46] The exchange-correlation functional was described by the Perdew, Burke, and Ernzerhof (PBE) parameterization of the generalized gradient approximation (GGA).[47-48] A cutoff energy of 400 eV was employed for the plane-wave basis set of all calculations. The metallic Pd was mimicked with a (6 × 6 × 4) Pd(111) slab. The partially hydrogenated Pd was modelled with the aforementioned Pd(111) surface with 9 H atom adsorbed at the hollow sites. This structure is referred to as the $Pd_{36}H_9$ in this work. The PdO catalyst was modelled with a PdO(101) slab, consisting of 120 Pd and 120 O atoms. During structural optimizations, only the top two periodic layers were allowed to relax in three dimensions, and the bottom two layers were restricted. Ten relaxed ethanol molecules were added to fill the vacuum region close to the Pd-based surfaces to mimic the liquid ethanol solvent. The structure relaxation was reached until the residual force was below 0.01 eV $Å^{-1}$. The Brillouin zone was sampled by a 2 × 2 × 1 k-point sampling for the periodic Pd-based surface models and a 1 × 1 × 1 k-point sampling for isolated molecules. All periodic surface models were placed in cubic supercells with lattice parameter c = 30 Å in the z direction to avoid interactions between periodic images. An empirical correlation (DFT-D3) was employed to describe the van der Waals interactions.[49] The adsorption energies of molecules on the various Pd-based surfaces were calculated according to the following equation:

$$E_{ads} = E(\text{adsorbed system}) - E(\text{desorbed system}) \qquad \text{Eq. 1}$$

The change of the Gibbs free energy (ΔG) for each elementary step at the zero potential were calculated using the following equation:

$$\Delta G = \Delta E + \Delta E_{ZPE} - T\Delta S \qquad \text{Eq. 2}$$

where E was the total energy obtained directly from the DFT calculations. E_{ZPE} and S were the zero-point energy and the entropy, respectively. T was the temperature (298.15 K).

Synthesis of the catalyst. The following commercial precursors were applied: Melamine monomer and cyanuric acid (98.0%, TCI Shanghai Co. Ltd.); $PdCl_2$ (analytic grade, Shanghai Aladdin Bio-Chem Technology Co. Ltd.); NaOH (97%, Saen Chemical Technology Co. Ltd.); $NaBH_4$ (analytic grade, Alfa Aesar (China) Chemical Co. Ltd.). All chemicals were used as received without further purification.

The graphitic carbon nitride (CN): The CN was synthesized by a thermal condensation method according to the literature.[48] Melamine monomer (1 g) and cyanuric acid (5 g) powders were loaded in a crucible with a lid and calcined in a muffle oven at 550 °C for 4 h using a ramping rate of 5 °C·min^{-1} and then cooled to room temperature (RT) naturally.

Pd(II)/CN: A modified photo-deposition method was utilized to prepare the Pd(II)/CN. Firstly, 0.4 g of CN and calculated amount of $PdCl_2$ (Pd loading: 3 wt%) were added in 15 mL of absolute ethanol (99.7 vol%), sonicated for 0.5 h to obtain a homogenous suspension. After sonication, 10 mL DI water was added into the 15 mL suspension, which was deaerated by N_2 purging for three times under magnetic stirring. A LED (410 nm, 150 mW) lamp was then employed to irradiate the suspension at RT for 5 h under deaerated conditions. The Pd(II)/CN suspension was centrifuged and washed with DI water and ethanol for 3 times, and finally the powders were dried in a vacuum oven at 60 °C for 12 h.

PdH_X/CN: A modified photo-deposition method was utilized to prepare the PdH_X/CN. Firstly, 0.4 g of CN and calculated amount of $PdCl_2$ (Pd loading: 3 wt%) were added in 25 mL of absolute ethanol (99.7 vol%), sonicated for 0.5 h to obtain a homogenous suspension. The suspension was deaerated by Ar purging for three times under magnetic stirring. A LED (410 nm, 150 mW) lamp was then employed to irradiate the suspension at RT for 10 h under deaerated conditions. The PdH_X/CN suspension was centrifuged and washed with DI water and ethanol for 3 times, and finally the powders were dried in a vacuum oven at 60 °C for 12 h.

Characterization of the catalyst. The surface chemical compositions of the samples and oxidation states of each element were investigated using an X-ray photoelectron spectrometer (PHI 5000 VersaProbe Ⅲ, ULVAC-PHI) equipped with a monochromatic Al Kα X-ray source. Survey scans were measured using the following parameters: energy scan range of 1200 to -10 eV, pass energy of 160 eV, dwell time of 0.1 s, step size of 1 eV, and scan numbers of 3 times. For the region-of-interest spectra (C1s, N1s, Pd3d and O1s), a pass energy of 40 eV and a step size of 0.1 eV with a dwell time of 0.5 s were utilized. Adventitious C (C1s = 284.6 eV) was employed for calibration.

The Brunauer-Emmett-Teller (BET) surface area of samples was obtained by the nitrogen adsorption/desorption isotherms measured at 77 K on a Micromeritics TriStar Ⅱ 3020 system. PXRD data were collected on a Bruker D8 Advance diffractometer equipped with a Cu anode (40 kV, 40 mA). The PXRD patterns were recorded in the scan range of 10-80°, a step size of 0.02° and a dwell time of 0.5 s. For the fine diffraction pattern, a scan range of 37-41°, a step size of 0.01° and a dwell time of 5 s. The microstructural information of the photocatalyst was studied using a transmission electron microscope (FEI Titan ThemisZ) operated at 120 kV. The sample was added into 1 mL of alcohol and sonicated for 5 min to form a suspension. A drop of the suspension was cast on the Cu stage and dried in air. The radical species generated during the photocatalytic reduction of benzaldehyde were analyzed by EPR using an X-band JES-X320 spectrometer in the range of 321-331 mT at RT. A modulation width of 0.14 mT and an amplitude of 200 was used for all measurements. The 5,5-dimethyl-1-pyrroline N-oxide (DMPO) was utilized as the spin-trapping reagent.

TPD-MS was utilized to analyze the adsorption of benzaldehyde and acetal on Pd(II)/CN and PdHX/CN using a chemisorption analyzer (AutoChem II) coupled with a MS (OmniStar GSD, Pfeiffer). The process is as the following: Firstly, fresh photocatalyst powders (30 mg) were placed in a closed chamber and purged with Ar gas for 30 minutes to ensure a clean surface of the photocatalyst. Then the organic compounds (5 mL) were introduced to the photocatalyst chamber for 1 h via Ar purging. Next, the inlet valve was closed and the photocatalyst were kept in organic compound/Ar atmosphere for another 6 h. Finally, the photocatalyst powders were loaded into a U-shaped quartz tube in a chemisorption analyzer. To start the TPD test the loaded sample was heated to 500 ^{o}C at a ramp rate of 10 $^{o}C\cdot min^{-1}$ with a He flow rate of 50 $mL\cdot min^{-1}$. Meanwhile the desorbed gases were monitored by the coupled MS in real time.

Catalytic performance. The photocatalytic conversion of aromatic carbonyls was performed in a multichannel reaction system with six Pyrex-glass-made reactors (SUNCAT INSTRUMENTS, China). The setup consists of three parts: A circular 410 nm LED light source with magnetic stir base, a DC power supply, and a cooling system for the light source. Each of the reactor contains 2 mL of alcohol with 10 mg photocatalyst and 10 mM reactant, which was purged and filled with Ar before irradiation. Details of the reaction system can be found in our previous work.[23] After reaction, the suspension was centrifuged and the aliquots were analyzed by gas chromatography (Agilent GC 8860) and combined gas chromatography and mass spectrometry (GC-MS, Agilent 8860 GC system coupled with a 5977B mass selective detector). An HP-5 MS column and an FID detector were equipped in the GC-MS.

The evolution of gas phase products was monitored by a quadruple mass spectrometer (MS, HPR-20, Hiden) equipped with an *in-situ* reactor. In this reaction system, a reaction chamber with a quartz window was connected to the mass spectrometer via a leak-valve. The analysis was carried out using a reaction mixture that consists of 50 mg photocatalyst and 10 mM benzaldehyde in 10 mL ethanol. Control experiments in the absence of benzaldehyde were also performed for comparison. Before irradiation, the reactor was evacuated and then filled with Ar gas. A purple LED (410 nm, 350 mW) was utilized as the light source to match the light intensity that is used for photocatalytic conversion of aromatic carbonyls (14.8 $mW\cdot cm^{-2}$). The light intensity for all experiments was determined using an optical power meter (Thorlabs PM125D) equipped with a thermal sensor (0.002-10 W), which is aligned to the center of the light source at experimental distances.

ASSOCIATED CONTENT

Supporting Information. Detailed synthesis and additional characterizations of the catalyst, calculation modeling, and catalytic performances are available online for free.

AUTHOR INFORMATION

Corresponding Author

* Emails: suren@suda.edu.cn (RS); hplin@snnu.edu.cn (HL)

Author Contributions

The manuscript was written through contributions of all authors. ‡These authors contributed equally.

ACKNOWLEDGMENT

RS would like to thank the NSFC (projects number: 21972100), the Project of Innovation and Entrepreneurship of Jiangsu Province (grant number: JSSCRC202010539), the Suzhou Foreign Academician Workstation (project number: SWY2022001) for financial support. HL acknowledge financial supports from the Fundamental Research Funds for the Central Universities (GK202203002).

REFERENCES

1. Fu, J.; Lym, J.; Zheng, W.; Alexopoulos, K.; Mironenko, A. V.; Li, N.; Boscoboinik, J. A.; Su, D.; Weber, R. T.; Vlachos, D. G., C–O bond activation using ultralow loading of noble metal catalysts on moderately reducible oxides. *Nat. Catal.* **2020,** *3* (5), 446-453.
2. Moos, G.; Emondts, M.; Bordet, A.; Leitner, W., Selective hydrogenation and hydrodeoxygenation of aromatic ketones to cyclohexane derivatives using a Rh@ SILP catalyst. *Angew. Chem. Int. Ed.* **2020,** *59* (29), 11977-11983.
3. Asensio, J. M.; Miguel, A. B.; Fazzini, P. F.; Van Leeuwen, P. W.; Chaudret, B., Hydrodeoxygenation Using Magnetic Induction: High - Temperature Heterogeneous Catalysis in Solution. *Angew. Chem. Int. Ed.* **2019,** *131* (33), 11428-11432.
4. Sullivan, M. M.; Bhan, A., Acetone hydrodeoxygenation over bifunctional metallic–acidic molybdenum carbide catalysts. *ACS Catal.* **2016,** *6* (2), 1145-1152.
5. Kuai, L.; Chen, Z.; Liu, S.; Kan, E.; Yu, N.; Ren, Y.; Fang, C.; Li, X.; Li, Y.; Geng, B., Titania supported synergistic palladium single atoms and nanoparticles for room temperature ketone and aldehydes hydrogenation. *Nat. Commun.* **2020,** *11* (1), 48.
6. Frei, M. S.; Mondelli, C.; Garcia-Muelas, R.; Kley, K. S.; Puertolas, B.; Lopez, N.; Safonova, O. V.; Stewart, J. A.; Curulla Ferre, D.; Perez-Ramirez, J., Atomic-scale engineering of indium oxide promotion by palladium for methanol production via CO_2 hydrogenation. *Nat. Commun.* **2019,** *10* (1), 3377.
7. Zhao, M.; Yuan, K.; Wang, Y.; Li, G.; Guo, J.; Gu, L.; Hu, W.; Zhao, H.; Tang, Z., Metal–organic frameworks as selectivity regulators for hydrogenation reactions. *Nature* **2016,** *539* (7627), 76-80.
8. Zhang, B.; Sun, G.; Ding, S.; Asakura, H.; Zhang, J.; Sautet, P.; Yan, N., Atomically Dispersed Pt1-Polyoxometalate Catalysts: How Does Metal-Support Interaction Affect Stability and Hydrogenation Activity? *J. Am. Chem. Soc.* **2019,** *141* (20), 8185-8197.
9. Kahsar, K. R.; Schwartz, D. K.; Medlin, J. W., Control of metal catalyst selectivity through specific noncovalent molecular interactions. *J. Am. Chem. Soc.* **2014,** *136* (1), 520-526.
10. Wu, X.; Li, J.; Xie, S.; Duan, P.; Zhang, H.; Feng, J.; Zhang, Q.; Cheng, J.; Wang, Y., Selectivity Control in Photocatalytic Valorization of Biomass-Derived Platform Compounds by Surface Engineering of Titanium Oxide. *Chem* **2020,** *6* (11), 3038-3053.
11. Tian, S.; Wang, B.; Gong, W.; He, Z.; Xu, Q.; Chen, W.; Zhang, Q.; Zhu, Y.; Yang, J.; Fu, Q.; Chen, C.; Bu, Y.; Gu, L.; Sun, X.; Zhao, H.; Wang, D.; Li, Y., Dual-atom Pt heterogeneous catalyst with excellent catalytic performances for the selective hydrogenation and epoxidation. *Nat. Commun.* **2021,** *12* (1), 3181.
12. Landry, M. J.; Gellé, A.; Meng, B. Y.; Barrett, C. J.; Moores, A., Surface-Plasmon-Mediated Hydrogenation of Carbonyls Catalyzed by Silver Nanocubes under Visible Light. *ACS Catal.* **2017,** *7* (9), 6128-6133.
13. Hao, C. H.; Guo, X. N.; Pan, Y. T.; Chen, S.; Jiao, Z. F.; Yang, H.; Guo, X. Y., Visible-Light-Driven Selective Photocatalytic Hydrogenation of Cinnamaldehyde over Au/SiC Catalysts. *J. Am. Chem. Soc.* **2016,** *138* (30), 9361-4.
14. Guo, M.; Jayakumar, S.; Luo, M.; Kong, X.; Li, C.; Li, H.; Chen, J.; Yang, Q., The promotion effect of π-π interactions in Pd NPs catalysed selective hydrogenation. *Nat. Commun.* **2022,** *13* (1), 1770.
15. Huang, Y.; Liu, Z.; Gao, G.; Xiao, Q.; Martens, W.; Du, A.; Sarina, S.; Guo, C.; Zhu, H., Visible light-driven selective hydrogenation

of unsaturated aromatics in an aqueous solution by direct photocatalysis of Au nanoparticles. *Catal. Sci. Technol.* **2018,** *8* (3), 726-734.
16. Wang, Y.; Liu, X.-H.; Wang, R.; Cula, B.; Chen, Z.-N.; Chen, Q.; Koch, N.; Pinna, N., Secondary phosphine oxide functionalized gold clusters and their application in photoelectrocatalytic hydrogenation reactions. *J. Am. Chem. Soc.* **2021,** *143* (25), 9595-9600.
17. Fang, W.; Riisager, A., Efficient valorization of biomass-derived furfural to fuel bio-additive over aluminum phosphate. *Appl. Catal. B* **2021,** *298*, 120575.
18. Tamura, Y.; Kanomata, K.; Kitaoka, T., Interfacial Hydrolysis of Acetals on Protonated TEMPO-oxidized Cellulose Nanofibers. *Sci. Rep.* **2018,** *8* (1), 5021.
19. Myles, L.; Gore, R.; Špulák, M.; Gathergood, N.; Connon, S. J., Highly recyclable, imidazolium derived ionic liquids of low antimicrobial and antifungal toxicity: A new strategy for acid catalysis. *Green Chem.* **2010,** *12* (7), 1157-1162.
20. Beltran, F.; Bergamaschi, E.; Funes-Ardoiz, I.; Teskey, C. J., Photocontrolled Cobalt Catalysis for Selective Hydroboration of alpha,beta-Unsaturated Ketones. *Angew. Chem. Int. Ed.* **2020,** *59* (47), 21176-21182.
21. Li, H.; Gao, Z.; Lei, L.; Liu, H.; Han, J.; Hong, F.; Luo, N.; Wang, F., Photocatalytic transfer hydrogenolysis of aromatic ketones using alcohols. *Green Chem.* **2020,** *22* (12), 3802-3808.
22. Koh, K.; Sanyal, U.; Lee, M. S.; Cheng, G.; Song, M.; Glezakou, V. A.; Liu, Y.; Li, D.; Rousseau, R.; Gutiérrez, O. Y., Electrochemically tunable proton - coupled electron transfer in Pd - catalyzed benzaldehyde hydrogenation. *Angew. Chem. Int. Ed.* **2020,** *132* (4), 1517-1521.
23. Kohtani, S.; Yoshioka, E.; S, Kenji.; Kudo, A.; Miyabe, H., Adsorptive and Kinetic Properties on Photocatalytic Hydrogenation of Aromatic Ketones upon UV Irradiated Polycrystalline Titanium Dioxide: Differences between Acetophenone and Its Trifluoromethylated Derivative. *J. Phys. Chem. C* **2012,** *116* (33), 17705-17713.
24. Lv, D. D.; Li, Y. R.; Qiao, W.; Zhang, D. D.; Mai, Y. Q.; Cai, N. J.; Xiang, H. W.; Li, Y. W.; Niemantsverdriet, H.; Hao, W. C.; Su, R., Metal cocatalyst mediated photocatalytic dehydrogenative-condensation and direct condensation cross-coupling of aniline and alcohol. *Appl. Catal. B* **2022,** *309*, 121264.
25. Guo, Y.; Huang, Y.; Zeng, B.; Han, B.; Akri, M.; Shi, M.; Zhao, Y.; Li, Q.; Su, Y.; Li, L.; Jiang, Q.; Cui, Y. T.; Li, L.; Li, R.; Qiao, B.; Zhang, T., Photo-thermo semi-hydrogenation of acetylene on Pd1/TiO2 single-atom catalyst. *Nat. Commun.* **2022,** *13* (1), 2648.
26. Mori, K.; Sano, T.; Kobayashi, H.; Yamashita, H., Surface engineering of a supported PdAg catalyst for hydrogenation of CO_2 to formic acid: elucidating the active Pd atoms in alloy nanoparticles. *J. Am. Chem. Soc.* **2018,** *140* (28), 8902-8909.
27. Huang, F.; Deng, Y.; Chen, Y.; Cai, X.; Peng, M.; Jia, Z.; Ren, P.; Xiao, D.; Wen, X.; Wang, N., Atomically dispersed Pd on nanodiamond/graphene hybrid for selective hydrogenation of acetylene. *J. Am. Chem. Soc.* **2018,** *140* (41), 13142-13146.
28. Ueno, T.; Suzuki, M.; Goto, T.; Matsumoto, T.; Nagayama, K.; Watanabe, Y., Size- selective olefin hydrogenation by a Pd nanocluster provided in an apo- ferritin cage. *Angew. Chem. Int. Ed.* **2004,** *43* (19), 2527-2530.
29. Zhao, Z.; Bababrik, R.; Xue, W.; Li, Y.; Briggs, N. M.; Nguyen, D.-T.; Nguyen, U.; Crossley, S. P.; Wang, S.; Wang, B., Solvent-mediated charge separation drives alternative hydrogenation path of furanics in liquid water. *Nat. Catal.* **2019,** *2* (5), 431-436.
30. Yu, J.; Liu, Q.; Qiao, W.; Lv, D.; Li, Y.; Liu, C.; Yu, Y.; Li, Y.; Niemantsverdriet, H.; Zhang, B.; Su, R., Catalytic Role of Metal Nanoparticles in Selectivity Control over Photodehydrogenative Coupling of Primary Amines to Imines and Secondary Amines. *ACS Catal.* **2021,** *11* (11), 6656-6661.
31. Jin, X.; Li, C.; Xu, C.; Guan, D.; Cheruvathur, A.; Wang, Y.; Xu, J.; Wei, D.; Xiang, H.; Niemantsverdriet, J. W.; Li, Y.; Guo, Q.; Ma, Z.; Su, R.; Yang, X., Photocatalytic CC bond cleavage in ethylene glycol on TiO2: A molecular level picture and the effect of metal nanoparticles. *J. Catal.* **2017,** *354*, 37-45.
32. Niu, Y.; Liu, X.; Wang, Y.; Zhou, S.; Lv, Z.; Zhang, L.; Shi, W.; Li, Y.; Zhang, W.; Su, D. S., Visualizing formation of intermetallic PdZn in a palladium/zinc oxide catalyst: Interfacial fertilization by PdHx. *Angew. Chem. Int. Ed.* **2019,** *58* (13), 4232-4237.
33. Jia, Y.; Huang, T.-H.; Lin, S.; Guo, L.; Yu, Y.-M.; Wang, J.-H.; Wang, K.-W.; Dai, S., Stable Pd–Cu Hydride Catalyst for Efficient Hydrogen Evolution. *Nano Lett.* **2022,** *22* (3), 1391-1397.
34. García-Gabaldón, M.; Pérez-Herranz, V.; García-Antón, J.; Guiñón, J. L., Electrochemical study of the activating solution for electroless plating of polymers. *J. Appl. Electrochem.* **2007,** *37* (10), 1145-1152.
35. Sarac, B.; Karazehir, T.; Mühlbacher, M.; Kaynak, B.; Gammer, C.; Schöberl, T.; Sarac, A. S.; Eckert, J., Electrosorption of Hydrogen in Pd-Based Metallic Glass Nanofilms. *ACS Appl. Energy Mater.* **2018,** *1* (6), 2630-2646.
36. Zhan, C.; Li, H.; Li, X.; Jiang, Y.; Xie, Z., Synthesis of PdH0.43 nanocrystals with different surface structures and their catalytic activities towards formic acid electro-oxidation. *Sci. China Mater.* **2019,** *63* (3), 375-382.
37. Sarac, B.; Ivanov, Y. P.; Karazehir, T.; Mühlbacher, M.; Kaynak, B.; Greer, A. L.; Sarac, A. S.; Eckert, J., Ultrahigh hydrogen-sorbing palladium metallic-glass nanostructures. *Mater. Horiz.* **2019,** *6* (7), 1481-1487.
38. Zhang, J.; Chen, M.; Li, H.; Li, Y.; Ye, J.; Cao, Z.; Fang, M.; Kuang, Q.; Zheng, J.; Xie, Z., Stable palladium hydride as a superior anode electrocatalyst for direct formic acid fuel cells. *Nano Energy* **2018,** *44*, 127-134.
39. Rose, A.; Maniguet, S.; Mathew, R. J.; Slater, C.; Yao, J.; Russell, A. E., Hydride phase formation in carbon supported palladium nanoparticle electrodes investigated using in situ EXAFS and XRD. *Phys. Chem. Chem. Phys.* **2003,** *5* (15).
40. Khanuja, M.; Mehta, B.; Agar, P.; Kulriya, P.; Avasthi, D., Hydrogen induced lattice expansion and crystallinity degradation in palladium nanoparticles: Effect of hydrogen concentration, pressure, and temperature. *J. Appl. Phys.* **2009,** *106* (9), 093515.
41. Chorkendorff, I and Niemantsverdriet, J.W., Concepts of Modern Catalysis and Kinetics, 3rd Ed., Wiley-VCH, Weinheim, **2017**, 41-48.
42. Zhang, H.; Zhang, W.; Zhao, M.; Yang, P.; Zhu, Z., A site-holding effect of TiO2 surface hydroxyl in the photocatalytic direct synthesis of 1,1-diethoxyethane from ethanol. *Chem. Commun.* **2017,** *53* (9), 1518-1521.
43. Kresse, G.; Furthmuller, J., Efficient iterative schemes for ab initio total-energy calculations using a plane-wave basis set. *Phys. Rev. B* **1996,** *54* (16), 11169-11186.
44. Kresse, G.; Furthmuller, J., Efficiency of ab-initio total energy calculations for metals and semiconductors using a plane-wave basis set. *Comput. Mater. Sci.* **1996,** *6* (1), 15-50.
45. Blochl, P. E., Projector Augmented-Wave Method. *Phys. Rev. B* **1994,** *50* (24), 17953-17979.
46. Kresse, G.; Joubert, D., From ultrasoft pseudopotentials to the projector augmented-wave method. *Phys. Rev. B* **1999,** *59* (3), 1758-1775.
47. Perdew, J. P.; Burke, K.; Ernzerhof, M., Generalized gradient approximation made simple. *Phys. Rev. Lett.* **1996,** *77* (18), 3865-3868.
48. Perdew, J. P.; Chevary, J. A.; Vosko, S. H.; Jackson, K. A.; Pederson, M. R.; Singh, D. J.; Fiolhais, C., Atoms, Molecules, Solids, and Surfaces - Applications of The Generalized Gradient Approximation for Exchange and Correlation. *Phys. Rev. B* **1992,** *46* (11), 6671-6687.
49. Grimme, S.; Antony, J.; Ehrlich, S.; Krieg, H., A consistent and accurate ab initio parametrization of density functional dispersion correction (DFT-D) for the 94 elements H-Pu. *J. Chem. Phys.* **2010,** *132* (15), 154104.

TOC